

A VISION SYSTEM WITH MULTIPLE SENSORS IN INTELLIGENT ROBOT AND PHOTOGRAMMETRIC CONTRIBUTIONS

Dr. Guoqing Zhou

Department of Civil & Environmental Engineering and Geodetic Science
The Ohio State University
470 Hitchcock Hall, 2070 Neil Avenue, Columbus, OH 43210-1275
Fax: +1 (0) 614 292-2957, Tel: +1 (0) 614 292-6683, Email: zhou.77@osu.edu

ISPRS Commission V, Working Group WG V/1

KEY WORDS: Vision system, Space robot, Multiple sensors, Camera calibration, Natural landmarks, 3D reconstruction CAD, Line photogrammetry.

ABSTRACT

For the purpose of providing sufficient and reliable vision information for Space Intelligent Robotic Manipulators, a vision system called *Space Intelligent Vision Equipment-SIVE* was developed. The paper firstly describes the SIVE outline including systemic design, SIVE function, hardware environment, software assembly line, algorithm (software) characters, then photogrammetric contributions to SIVE, including camera calibration using line features, CAD-based objects reconstruction using linear photogrammetry, are focused.

The camera calibration approach based on natural landmarks was used for SIVE. In the proposed scheme, three pairs of parallel straight lines are used to solve rotation parameters and internal parameters. The coordinates of a distinct feature point from 3-D to 2-D, together with a length of a line segment, are used to solve translation parameters of the camera.

CAD-based object reconstruction using line photogrammetry was used for SIVE. In this algorithm, assuming that an object in CAD is constructed by Boolean set operators of primitives (CSG), and each face is described by Boundary presentation (B-pre). Straight and curved lines and planar and curved surfaces in 3D space are described by parametric equations. In the mathematical model of reconstruction, we consider geometric elements as unknown parameters, and match images (2D) and objects (3D) directly. A lot of simulations and practical experiments were performed.

1. INTRODUCTION

Our vision research group (Dept. of Computer Science and Technology, Tsinghua University) was fulfilling a project of a vision system design for the Chinese Aerospace Industrial Department. The aim of system is to provide sufficient and reliable vision information for Experimental Testbed of Space Intelligent Robotic Manipulators. We call this system *Space Intelligent Vision Equipment -SIVE*.

The SIVE is required to 1) recognize and locate CAD-based objects and obstructions in space; 2) guide correctly robot to finish various operations including autonomous operation, master slave operation, share & traded operation and coordination of two arms operation; 3) provide enough vision information so that operator can interact the control system of robot; 4) provide the help for tele-operation with virtual reality.

Regarding the space environment, SIVE shows following characters besides common ones of machine vision:

1. Micro-gravity, long time-delay, vacuum, no uniform light, and drift (instability) object.

2. SIVE can implement autonomous operation, master slave operation, share & traded operation and two-arm coordination operation.

3. SIVE can provide helpfulness for tele-operation by means of virtual reality.

4. SIVE has higher robust and reliability since it almost is impossible (very difficult) to repair and to change equipment due to far distance between airborne and earth.

In so huge a vision system, I, as a unique photogrammetrist, participated in the project. I would like to present it to photogrammetrists, especially close-range photogrammetrists, so as to let many colleagues know of that photogrammetry can play a large role in robot vision/computer vision.

This paper firstly describes the SIVE outline, and then photogrammetric contributions, including camera calibration using line features and CAD-based object reconstruction using line photogrammetry, are focused.

2. OUTLINE of SIVE SYSTEM

SIVE consists of two PUMA/560 robot arms, six CCD cameras and three programmable structural lights. Each arm is mounted on a moving platform; each platform has a tilt and rotation capability and can move along a two rail linear track. Two wide angle CCD cameras of six are mounted on ceiling so as to obtain spread view. Each pair of cameras is mounted on robotic arm respectively, each programmable structural light controlled by computer is mounted in the middle of stereo cameras in order to obtain accurate position, and increase robust of three-dimensional information when using passive and active vision. As illustrated in Fig. 1. The proposed hardwares of SIVE are composed of as follows [see figure 2]:

1. Cameras and structural light source;
2. Image grabber and low level image processor;
3. Visual information fusion and image understanding;
4. Visual information output and display.

2.1 Cameras

How to select the camera types (such as focal length, field angle) and how to arrange cameras' position with considering precision of object location, space environment, systemic reliability, robotic operations, information fusion, and so on, are seriously discussed by our research group. The final decision is: 1) two wide angle video cameras (model JE2362, black and white Javelin cameras) are mounted on the ceiling above (see cameras 1, 2 in Fig. 1) so as to provide a general view of robotic

work space; 2) two Toshiba micro-miniature remote sense-head black and white CCD video cameras (model IK-M30M) are mounted on robotic arms so as to precisely locate objects; 3) the eye-hand configuration is used to provide dynamic 3-D vision for the testbed system (Fig 1) [Yu 1995].

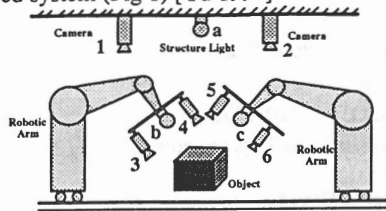


Fig. 1. SIVE system outline.

2.2 Structural light resource

The robotic testbed fixed on the ceiling above is a laser scanning system made by General Scanning, Inc. (model EDK 500M), and the laser is an Uniphase 5 mW HeNe laser (model 1125P). The scanning of the laser is controlled by a SUN/4 workstation. The SUN/4 can program the orientation of the laser scanning according to prediction and hypothesis of object location. The laser scanner is used to solve image correspondence problem in 3-D vision. It also provides structural light patterns (such as point, line) which are used as an additional means to understand 3-D objects.

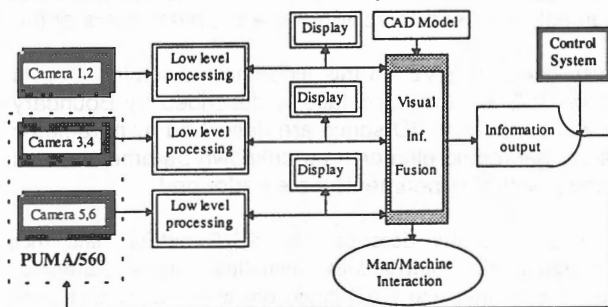


Fig. 2. SIVE flow scheme.

2.3 Low level processing in SIVE

In order to increase speed, we divide image processing into low and high level processing. Two parts can simultaneously work. The information from six cameras is processed using a high speed vision system made by Datacube, Inc. The Datacube vision system can receive information from any two of six cameras simultaneously, and can operate at real-time. It is controlled by a SUN/4 workstation. Multiple views from six cameras are used to provide enough information in order to identify the objects, which can not correctly be recognized by a single view. Up to now, it can finish the following functions:

- Camera calibration and structural light plane calibration;
- Real-time image display and multi-bus exchange;
- Gray histogram statistics;
- Edge detection;
- Image segmentation;
- Image morphology operating;
- Optic flow computing.

2.4 Information fusion for image understanding

Information fusion is implemented by a Silicon Graphics Indigo 2. This module has at present following functions:

- CAD-based object recognition in space;
- Object location and pose determination;
- To determine and to predicate relative the position between robotic arms and objects;
- Virtual environment generation;

- To extract useful vision information, and to convey it into control system.

3. ALGORITHM CHARACTERS in SIVE

3.1 Four kinds of operations

SIVE should support four kinds of operators as follows:

In a master slave operation, SIVE works through a control command from operator. The operator may decide how to acquire vision information necessary, how to arrange program to run, how to implement task. Therefore, the main purpose of SIVE is to provide a monitor/display for operator. In this case, VR is used to predict the display.

In share & traded operations, operator implements object recognition. The operator finds an object on the monitor, and input the number of the object and gives the initial position with mouse, and then SIVE can locate the object. In addition, due to knowing CAD model, SIVE can determine object location using feature-based model match.

In autonomous operation, the system can automatically recognize and locate CAD-based objects. Of course, the models of objects are considered as prior knowledge.

In coordination operation of two arms, SIVE only provides information necessary for one arm, and other arms are considered as obstruction.

3.2 VR Technique

How to keep up consistency between the virtual and realistic environments is an important topic in SIVE. We studied a virtual visual model, renewal virtual environmental model at real-time [Yu 1995]. SIVE can now generate 3-D virtual environment so as to provide intuitive depth information for the operator. The operators wearing a pair of crystal stereo glasses can perceive the position of objects and robotic arms from various directions. SIVE can still help the operator to get rid of long time-delay.

3.3 Increasing reliability of SIVE

In order to increase reliability and robustness, multi-strategies for object recognition and location are adopted. For example, a combination of binocular passive vision and monocular active vision. Visual information fusion is also considered as a means of increasing reliability and robustness. In information fusion, we abide by such a rule: local visual information provided by active vision is most reliable, but visual information provided by cameras (1, 2) is most reliable when determining object position in a world coordination system.

3.4 Tracking drift objects

Tracking drift objects in space is very difficult since both drift objects and cameras change not only in position but also in pose. These changes are difficult to predict. Deformation contour tracking algorithm is adopted in SIVE.

4. PHOTOGRAMMETRIC CONTRIBUTIONS to SIVE

In SIVE, photogrammetric contributions include 1) calibrating two cameras mounted on ceiling using line features; 2) calibrating a single camera and structural light (mounted on the robotic arms) plane using structural light technique; 3) transforming the relation between the end effector of the robotic arm and single camera, also called *eye-hand system calibration*; 4) reconstructing CAD-based objects using line photogrammetric technique. I here focus on 1) and 4).

4.1 Camera calibration using straight line features

In most previous calibration methods, artificial landmarks, (called *control points*), are required. However in space robot vision, it is not suitable to lay artificial landmarks for dynamic

SIVE environment, and it is also very difficult to find 3D and 2D corresponding points. We have to adopt straight lines instead of points as our feature landmark, and utilize geometric information of the straight lines to realize the camera calibration. The reasons selecting the straight line as landmark are:

- The straight line is a common, important natural landmark;
- The straight line is most easily detected than the point;
- The straight line contains a lot of important geometric information, such as parallel, orthogonal, intersection at a point.
- The straight line can be found in many objects, such as building, robot arm, industrial parts, cone, polyhedron.

A) Camera calibration model

Without considering optical distortion, the camera model is really a pinhole model. As shown in Fig. 3. Assuming that (x, y, z) present the coordinates of a visible point P in a fixed reference system $O-XYZ$, and (x_c, y_c, z_c) represent the coordinates of the same point in a camera-centered coordinate system $O_c-x_c y_c z_c$ [Fig. 3]. The origin of the camera-centered coordination system coincides with its optical axis, the image plane, which corresponds to the image sensing array, is assumed to be parallel to the (x_c, y_c) plane, f represents a (effective) focal length of the camera. The relationship between the world and the camera-centered coordinate systems is given by

$$\begin{pmatrix} x \\ y \\ z \end{pmatrix} = \lambda R \begin{pmatrix} x_c \\ y_c \\ z_c \end{pmatrix} + T \quad (1)$$

Where $R = (a_i, b_i, c_i)^T$, $i=1,2,3$ is a rotation matrix defining the camera orientation, λ is a scale factor, $T = (t_i)^T$, $i=1,2,3$ is a translation vector defining the camera position.

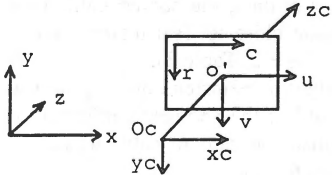


Fig. 3. Camera calibration model.

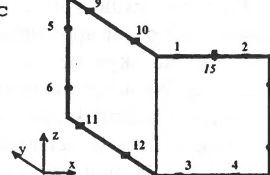


Fig. 4. Camera calibration using straight line groups [Feng 1986].

We now define, in image plane, the original coordinate system (O', u, v) , where O' represents the principal point of the image plan and the u and v axes are chosen parallel to the x_c and y_c axes. The image plane coordinates of the point P are given by following equations [Feng 1986]

$$\begin{aligned} u &= -f \frac{x}{z} \\ v &= -f \frac{y}{z} \end{aligned} \quad (2)$$

If (r, c) are used to represent the coordinates of pixels in the digital image plane with row, column, and (r_o, c_o) represents the row and column of the principal point o' in the image plane. Equation (2) may be represented by

$$\begin{aligned} r - r_o &= s_u u = -f s_u \frac{x}{z} = -f_u \frac{x}{z} \\ c - c_o &= s_v v = -f s_v \frac{y}{z} = -f_v \frac{y}{z} \end{aligned} \quad (3)$$

Where s_u, s_v are scale factors of sensors array in horizontal and vertical directions. Equation (3) represents distortion-free camera model (also called *pinhole model*).

B) Resolution Strategies

B.1) Estimation of the rotation parameters

Let us suppose there are three pairs of parallel straight lines in objective space (Fig. 4). Line 1-2 is parallel to line 3-4, and further parallel to X axis in the world coordination system; line 5-6 is parallel to line 7-8, and further parallel to Z axis; line 9-10 is parallel to line 11-12, and further parallel to Y axis.

For any a point on line 1-2, we can obtain the following equation from equation (1) and (2):

$$\frac{y - t_2}{z - t_3} = \text{constant } t$$

Supposing (u_1, v_1) and (u_2, v_2) are the projective coordinates of the point 1 and 2 in image plane respectively, then the above equation can be rewritten by:

$$(a_1 \ a_2 \ a_3) \begin{pmatrix} (v_2 - v_1)f \\ (u_1 - u_2)f \\ -w_1 \end{pmatrix} = 0 \quad w_1 = \begin{vmatrix} 1 & 1 & 1 \\ v_0 & v_1 & v_2 \\ u_0 & u_1 & u_2 \end{vmatrix} \quad (4)$$

where u_0, v_0 are the image coordinates of the principal point. In the same way, if (u_3, v_3) and (u_4, v_4) denote the position of the point 3 and 4 in the line 3-4, we can obtain

$$(a_1 \ a_2 \ a_3) \begin{pmatrix} (v_4 - v_3)f \\ (u_3 - u_4)f \\ -w_2 \end{pmatrix} = 0 \quad \begin{aligned} a_2 &= \frac{a_1(R_1 v_0 - P_1)}{a_1 + R_1 u_0} \\ a_3 &= \frac{a_1 R_1 f}{Q_1 + R_1 u_0} \end{aligned} \quad (5)$$

$$P_1 = \begin{vmatrix} v_2 - v_1 & 0 & 0 \\ 0 & u_3 & u_4 \\ 0 & v_3 & v_4 \end{vmatrix} - \begin{vmatrix} v_4 - v_3 & 0 & 0 \\ 0 & u_1 & u_2 \\ 0 & v_1 & v_2 \end{vmatrix} \quad (6)$$

$$Q_1 = \begin{vmatrix} u_3 - u_4 & 0 & 0 \\ 0 & v_1 & v_2 \\ 0 & u_1 & u_2 \end{vmatrix} - \begin{vmatrix} u_1 - u_2 & 0 & 0 \\ 0 & v_3 & v_4 \\ 0 & u_3 & u_4 \end{vmatrix}, \quad R_1 = \begin{vmatrix} u_1 - u_2 & u_3 - u_4 \\ v_1 - v_2 & v_3 - v_4 \end{vmatrix} \quad (7)$$

The orthogonal constrain of nine elements in rotation matrix R is given by

$$a_1^2 + a_2^2 + a_3^2 = 1 \quad (8)$$

Thus, we obtain the equation about a_1

$$a_1 = \frac{Q_1 + R_1 u_0}{D_1} \quad D_1 = \left[(Q_1 + R_1 u_0)^2 + (P_1 - R_1 v_0)^2 + (R_1 f)^2 \right]^{1/2} \quad (9)$$

Similarly, we can obtain the relations between the angle parameters (b_1, b_2, b_3) and the parallel straight line 9-10 and 11-12, which are parallel to Y axis, as well as the (c_1, c_2, c_3) and the parallel straight line 5-6 and line 7-8, which are parallel to Z axis.

$$b_1 = \frac{Q_2 + R_2 u_0}{D_2}, \quad b_2 = \frac{R_2 v_0 - P_2}{D_2}, \quad b_3 = \frac{R_2 f}{D_2} \quad (10)$$

$$c_1 = \frac{Q_3 + R_3 u_0}{D_3}, \quad c_2 = \frac{R_3 v_0 - P_3}{D_3}, \quad c_3 = \frac{R_3 f}{D_3} \quad (11)$$

Where: $P_2, Q_2, R_2, D_2, P_3, Q_3, R_3, D_3$ are similar to P_1, Q_1, R_1, D_1 .

B.2) Determination of the interior parameters (u_o, v_o, f)

Considering orthogonal constrain of the nine components in rotation matrix R , we obtain

$$\begin{pmatrix} -(Q_1 R_2 + Q_2 R_1) & (R_1 P_2 + R_2 P_1) & -R_1 P_2 \\ -(Q_3 R_1 - Q_1 R_3) & (R_3 P_1 + R_1 P_3) & -R_3 P_1 \\ -(Q_2 R_3 + Q_3 R_2) & (R_2 P_3 + R_3 P_2) & -R_3 P_2 \end{pmatrix} \begin{pmatrix} u_o \\ v_o \\ u_o^2 + v_o^2 + f^2 \end{pmatrix} = \begin{pmatrix} Q_1 Q_2 + P_1 P_2 \\ Q_3 Q_1 + P_3 P_1 \\ Q_2 Q_3 + P_2 P_3 \end{pmatrix} \quad (12)$$

B.3) Determination of the translation vector t

So far, we have known the rotate matrix $(R = (a_i, b_i, c_i), i = 1, 2, 3)$, the interior parameters (u_o, v_o, f) . If the length of

a straight line, and the coordinates for a point with 2D (u_m, v_m) and corresponding to 3D (x_M, y_M, z_M) are known, we can determine the translation vectors t using

$$T = \begin{pmatrix} x_M \\ y_M \\ z_M \end{pmatrix} - \lambda R \begin{pmatrix} x_c \\ y_c \\ z_c \end{pmatrix} = \begin{pmatrix} x_M \\ y_M \\ z_M \end{pmatrix} - \lambda R \begin{pmatrix} u_m \\ v_m \\ -f \end{pmatrix} \quad (13)$$

B.4) Distortions rectify

As a result of several types of imperfections in the design and assembly of lenses composing of the camera optical system, we think, generally speaking, that main distortion sources come from radial and discentering distortions, *i.e.*,

$$\delta_u(u, v) = \kappa_1 u(u^2 + v^2) + \rho_1(3u^2 + v^2) + 2\rho_2 uv$$

$$\delta_v(u, v) = \kappa_1 v(u^2 + v^2) + \rho_2(3u^2 + v^2) + 2\rho_1 uv \quad (14)$$

In order to rectify the distortions, we make full use of the geometric properties of straight lines. Provided that any a point 15 on the line 1-2 is selected, the points 1, 2 and 15 should be collinear in ideal case, *i.e.*, the area of triangle constructed by the points 1, 2 and 15 is zero (Fig. 4). In fact, owing to existing distortion, the three points are impossible to be strictly collinear. So, the collinear property of three points can be used to rectify the distortion, *i.e.*,

$$\begin{vmatrix} u'_1 + \delta(u'_1, v'_1) & v'_1 + \delta(u'_1, v'_1) & 1 \\ u'_2 + \delta(u'_2, v'_2) & v'_1 + \delta(u'_2, v'_2) & 1 \\ u'_{15} + \delta(u'_{15}, v'_{15}) & v'_1 + \delta(u'_{15}, v'_{15}) & 1 \end{vmatrix} \equiv 0 \quad (15)$$

It is easy to obtain the distortion parameters κ_1, ρ_1, ρ_2 values through solving (15).

C) Experiments and Analysis

Test 1: The first set of data is a simulated cube, whose coordinates of 3-D and corresponding to 2-D are designed by CAD, whose image is generated by back-projection (Fig. 5). The size of image is 200×200 pixels, and the sample distance is $50 \mu m$. The natural landmarks are edges of the cube, which strictly meet the conditions of our algorithm described above. The experimental results with four calibration methods are shown in Tab. 1. In selecting distortion parameters, we only considered radial distortion.

Test 2: A real image is chosen as experimental data, whose size is 512×512 pixels with $8^{bit}/256$ (Fig. 6). In order to compare the precision to be reached by using our approach with others. Edges with one pixel level accuracy are considered as natural landmarks. To other algorithms, we select corners, which are really an intersection point of two or more than straight lines, as distinct points. The experimental results with four calibration approaches are shown in Tab. 2.

Test 3: Another type of CCD camera (type: COSMICAR) was tested. A scene, which consists of many industrial parts, was grabbed when the camera was located with depth distance about 880mm long. The size of image is 512×512 pixels with $8^{bit}/256$ gray level. As illustrated Fig. 7. The experimental results with four calibration approaches are shown in Tab. 3.

Table 1

	Rotate Angle(°)			Position Par.(mm)		
	O	A	T	t1	T2	t3
Yakimov.	-0.664	0.904	0.663	234.711	-311.76	282.911
Tsai	-0.663	0.904	0.663	234.208	-311.89	282.345
DLT	-0.664	0.911	0.667	234.617	-311.85	282.773
Our Method	-0.666	0.909	0.669	234.437	-311.90	282.941
	Intrinsic Par. (pixel)			Distor. Par(10^{-6})		
	Uo	Vo	f	k1		
Yakimov.	103.2	100.8	320.3	-		
Tsai	101.8	101.7	320.6	5.6577		
DLT	103.6	102.5	320.1	1.951		

Our Method	102.9	100.4	320.7	4.8956 (*)
------------	-------	-------	-------	------------

Table 2

	Rotate Angle(°)			Position Par. (mm)		
	O	A	T	t1	T2	t3
Yakimov.	-0.193	15.451	0.838	-308.56	1276.51	-1275.51
Tsai	-0.188	15.613	0.843	-308.31	1276.03	-1275.55
DLT	-0.180	15.226	0.894	-308.48	1276.21	-1275.25
Our Method	-0.185	15.268	0.876	-308.32	1276.04	-1275.53
	Intrinsic Par. (pixel)			Dis. Par (10^{-6})		
	Uo	Vo	f	k1		
Yakimov.	255.91	251.05	1279.44	-		
Tsai	256.07	243.11	1273.45	19.655		
DLT	255.58	248.41	1281.04	24.813		
Our Method	255.94	241.79	1277.81	58.766(*)		

Table 3

	Rotate Angle(°)			Position Par. (mm)		
	O	A	T	t1	T2	t3
Yakimov.	0.32031	0.671134	-0.81435	620.1516	516.1162	825.9164
Tsai	0.31988	0.675613	-0.82147	621.0311	516.0393	825.5547
DLT	0.32180	0.669961	-0.81994	620.9882	516.1237	825.5553
Our Method	0.31895	0.668682	-0.81769	620.9824	516.0457	825.1373
	Intrinsic Par. (pixel)			Dis. Par (10^{-6})		
	Uo	Vo	f	k1		
Yakimov.	260.012	251.733	1614.44	-		
Tsai	257.973	253.622	1625.45	149.158		
DLT	251.584	258.017	1609.04	114.136		
Our Method	259.947	251.588	1617.81	258.563(*)		

(* The value of distortion parameter is a mean value of several lines)

D) Remarks and Conclusions

An approach for calibrating camera is proposed here. We result in following conclusions from experimental results:

- (1) From the result of simulation, the calibration parameters in our approach are close to others (Table 1).
- (2) From the result with the real data, the solved calibration parameters using our approach are close to Tsai method, and a little far Yakimovskyy method (Table 2, Table 3).

In a word, We adopt the straight lines instead of the points as our calibration landmarks, and utilize the geometric information of the straight lines to accomplish the camera calibration. The advantages can be summarized as follows:

- (a) Without known the equations of straight lines and coordinates of any control points, the interior and rotation parameters can be determined.
- (b) The computational process is linear, without any iteration and initiated values.
- (c) Orthogonal constrains about three axes are considered;
- (d) Distortions are rectified using straight line geometry.

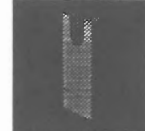


Fig. 5. Artificial image. Fig. 6. Real Image. Fig. 7. Real image.

4.2 GEMS-based Object Reconstruction Using LP

A) Representation of object in GEMS

SIVE is also required to locate and reconstruct 3D industrial objects. We developed a GEMS-based object reconstruction using line photogrammetry. So-called GEMS is a CAD system developed by CAD research group of department of computer science and technology at Tsinghua university (Sun 1989, 1990, Ren 1991). In GEMS, object representation is to combine CSG and Boundary represent (B-rep). CSG represents each complex object by geometric transformations (shift, rotation, and scale). Boolean set operators including two-tuple operators (intersection, merger, and difference), and mono-tuple operators

(rotation, scale transformation and transfer). This kind of representation can be illustrated by binary tree, whose leaves represent various primitives and whose nodes represent Boolean operator (Fig. 8).

This representation for primitives is concise, integrate and distinct. But its topologic relation is not clearly described. B-rep has a good effect in representing topologic relation of a complex object. In B-Pre, every object consists of finite surfaces, and every surface is enclosed by finite boundaries. Therefore, this representation is divided into volume, face, loops, edge and vertex. B-pre can also deposit geometric information and topology information in detail.

The geometric information, which indicates geometric characters of the point, line (curve) and face. For example, surface, such as sphere surface, is represented into $x = R \cos(\theta) \sin(\varphi)$, $y = R \sin(\theta) \sin(\varphi)$, $z = R \sin(\theta)$. The topologic information, which describes quantity, type and relation of the vertex, edge and face. Its purpose is to guarantee the object yielded is unique and legal.

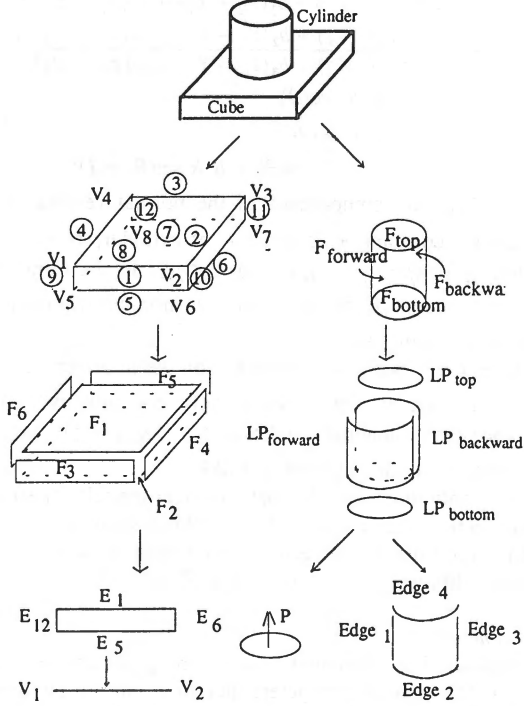


Fig. 9. Object representation with combination B-pre and CSG.

Our reconstruction method is based on this assumption that each industrial object is constructed by Boolean set operators of primitives, and each surface is described by B-pre. These line, curves, planar and curved surfaces in 3D space are described by parametric equations (Fig. 9).

In the following analysis it is assumed that the extraction and location of features in image space have already been accomplished and the correspondences between these features are established.

B) Mathematical model of reconstruction

In GEMS, an object is constructed by four coordination system transformations (Fig. 10). Assuming that T is a linear feature in scene (Fig. 11), and geometric elements (information) of this feature are expressed into

$$\begin{aligned} X &= X(\bar{s}) \\ Y &= Y(\bar{s}) \\ Z &= Z(\bar{s}) \end{aligned} \quad (16)$$

Where \bar{s} denotes the parameters to describe primitive including position parameters and geometric parameters. We also assume that linear features t , t' in the left and right image plan are perspective projection of the spatial linear feature T , and an arbitrary point P in the linear feature t is measured (Fig. 11), the collinearity equation can be formulated by the ray line pP .

$$x_p - x_o = -f \frac{a_1(X_p - X_s) + b_1(Y_p - Y_s) + c_1(Z_p - Z_s)}{a_3(X_p - X_s) + b_3(Y_p - Y_s) + c_3(Z_p - Z_s)} \quad (17a)$$

$$y_p - y_o = -f \frac{a_2(X_p - X_s) + b_2(Y_p - Y_s) + c_2(Z_p - Z_s)}{a_3(X_p - X_s) + b_3(Y_p - Y_s) + c_3(Z_p - Z_s)} \quad (17b)$$

In addition, the point P still meets the parametric equation describing the industrial object. *i.e.*

$$\begin{aligned} X_p &= X(\bar{s}) \\ Y_p &= Y(\bar{s}) \\ Z_p &= Z(\bar{s}) \end{aligned} \quad (18)$$

Where a_i , b_i , c_i , $i = 1, 2, 3$ are components of the rotation matrix for left image, X_s, Y_s, Z_s are coordinates of the perspective center of the image sensor, f denotes a constant of the image sensor, x_p, y_p denote the coordinates of the point P in image plane, X_p, Y_p, Z_p denote the coordinates of the point P .

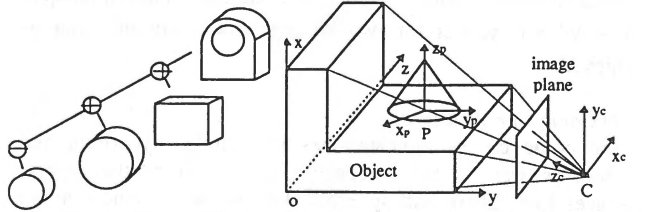


Fig. 8. CSG modeling. Fig. 10. Object and coordination system.

The mathematical model of reconstruction using line photogrammetry is formed by substituting the parametric equation (18) into the collinearity equation (17). We have

$$x_p - x_o = -f \frac{a_1(X_{P(\bar{s})} - X_s) + b_1(Y_{P(\bar{s})} - Y_s) + c_1(Z_{P(\bar{s})} - Z_s)}{a_3(X_{P(\bar{s})} - X_s) + b_3(Y_{P(\bar{s})} - Y_s) + c_3(Z_{P(\bar{s})} - Z_s)} \quad (19a)$$

$$y_p - y_o = -f \frac{a_2(X_{P(\bar{s})} - X_s) + b_2(Y_{P(\bar{s})} - Y_s) + c_2(Z_{P(\bar{s})} - Z_s)}{a_3(X_{P(\bar{s})} - X_s) + b_3(Y_{P(\bar{s})} - Y_s) + c_3(Z_{P(\bar{s})} - Z_s)} \quad (19b)$$

If an arbitrary point p' (non-correspondence with the point p) in feature t' is observed, the scene point P' corresponds to the point p' . The similar equation is formed.

$$x_{p'} - x_{o'} = -f' \frac{a'_1(X_{P'(\bar{s})} - X'_s) + b'_1(Y_{P'(\bar{s})} - Y'_s) + c'_1(Z_{P'(\bar{s})} - Z'_s)}{a'_3(X_{P'(\bar{s})} - X'_s) + b'_3(Y_{P'(\bar{s})} - Y'_s) + c'_3(Z_{P'(\bar{s})} - Z'_s)}$$

$$y_{p'} - y_{o'} = -f' \frac{a'_2(X_{P'(\bar{s})} - X'_s) + b'_2(Y_{P'(\bar{s})} - Y'_s) + c'_2(Z_{P'(\bar{s})} - Z'_s)}{a'_3(X_{P'(\bar{s})} - X'_s) + b'_3(Y_{P'(\bar{s})} - Y'_s) + c'_3(Z_{P'(\bar{s})} - Z'_s)} \quad (20)$$

Where a'_i , b'_i , c'_i , $i = 1, 2, 3$, X'_s, Y'_s, Z'_s , f' , $x_{p'}$, $y_{p'}$ for right image are similar parameters to left image. p' corresponds to scene point P' .

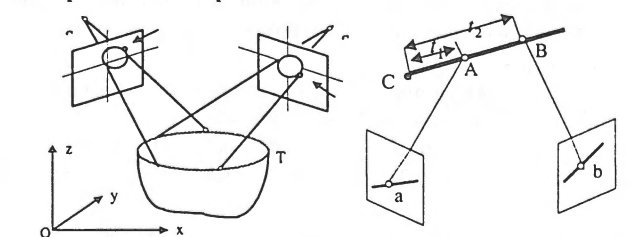


Fig. 11. Configure of LP reconstruction. Fig. 12. Straight line feature.

B.1) Straight line feature

The analytic equation for straight line can be expressed into

$$\bar{P} = \bar{C} + \bar{d} \cdot t \quad (21)$$

Where \bar{P} indicates an arbitrary observed point in straight line, $\bar{C} = (X_C, Y_C, Z_C)$ denotes a fixed point, t is a parameter.

Assuming that the point a and b in the left and right image planes are observed (a and b are non-correspondence points). The observation equation can be obtained.

left image:

$$\begin{aligned} x_a - x_a &= -f \frac{a_1(X_C + \alpha \cdot t_1 - X_S) + b_1(Y_C + \alpha \cdot t_1 - Y_S) + c_1(Z_C + \alpha \cdot t_1 - Z_S)}{a_3(X_C + \alpha \cdot t_1 - X_S) + b_3(Y_C + \alpha \cdot t_1 - Y_S) + c_3(Z_C + \alpha \cdot t_1 - Z_S)} \\ y_a - y_a &= -f \frac{a_2(X_C + \alpha \cdot t_1 - X_S) + b_2(Y_C + \alpha \cdot t_1 - Y_S) + c_2(Z_C + \alpha \cdot t_1 - Z_S)}{a_3(X_C + \alpha \cdot t_1 - X_S) + b_3(Y_C + \alpha \cdot t_1 - Y_S) + c_3(Z_C + \alpha \cdot t_1 - Z_S)} \end{aligned} \quad (22)$$

right image:

$$\begin{aligned} x_b - x_{a_2} &= -f' \frac{a'_1(X_C + \alpha \cdot t_2 - X'_S) + b'_1(Y_C + \alpha \cdot t_2 - Y'_S) + c'_1(Z_C + \alpha \cdot t_2 - Z'_S)}{a'_3(X_C + \alpha \cdot t_2 - X'_S) + b'_3(Y_C + \alpha \cdot t_2 - Y'_S) + c'_3(Z_C + \alpha \cdot t_2 - Z'_S)} \\ y_b - y_{a_2} &= -f' \frac{a'_2(X_C + \alpha \cdot t_2 - X'_S) + b'_2(Y_C + \alpha \cdot t_2 - Y'_S) + c'_2(Z_C + \alpha \cdot t_2 - Z'_S)}{a'_3(X_C + \alpha \cdot t_2 - X'_S) + b'_3(Y_C + \alpha \cdot t_2 - Y'_S) + c'_3(Z_C + \alpha \cdot t_2 - Z'_S)} \end{aligned} \quad (23)$$

Six fixative unknown parameters ($X_C, Y_C, Z_C, \alpha, \beta, \gamma$) and an additional unknown t or t' can be determined by the equations 22 and 23 for any a point. To the problem, the condition unequal $N + N' > 6$ is met for two images; unique solution can be achieved.

B.3) Conic Curve feature

The conic curves indicate ones like circle, hyperbola and ellipse, as well as the perspective projection of the regular surfaces like sphere and spheroid. Let us take a sphere as an example to construct the mathematical model.

Assuming that the model coordination system (describing sphere) is coincided with the spherical coordination system. An arbitrary measured point m in the left image is a respective projection of the point M in spherical surface. The collinearity equations can be formed by ray line mM . Moreover, the point M still meets the equation.

$$\begin{aligned} x &= R \sin(\varphi) \cos(\theta) \\ y &= R \sin(\varphi) \sin(\theta) \\ z &= R \cos(\varphi) \end{aligned} \quad (24)$$

Thus, we have (for the left image)

$$\begin{aligned} x_m - x_{a_1} &= -f \frac{a_1(R \sin(\varphi) \cos(\theta) - X_S) + b_1(R \sin(\varphi) \sin(\theta) - Y_S) + c_1(R \cos(\varphi) - Z_S)}{a_3(R \sin(\varphi) \cos(\theta) - X_S) + b_3(R \sin(\varphi) \sin(\theta) - Y_S) + c_3(R \cos(\varphi) - Z_S)} \\ y_m - y_{a_1} &= -f \frac{a_2(R \sin(\varphi) \cos(\theta) - X_S) + b_2(R \sin(\varphi) \sin(\theta) - Y_S) + c_2(R \cos(\varphi) - Z_S)}{a_3(R \sin(\varphi) \cos(\theta) - X_S) + b_3(R \sin(\varphi) \sin(\theta) - Y_S) + c_3(R \cos(\varphi) - Z_S)} \end{aligned} \quad (25)$$

Where R is a radius, φ, θ are the elevation and azimuth respectively. If another point e is observed, and the point E on the spherical surface corresponds to the point e , and the point M and the point E locate in the same hemisphere, the angle φ is invariable, and the angle θ is variable when the measured point is changed. If the point h is measured in the right image plan, the angles φ, θ differ from the point m , we have equation.

$$\begin{aligned} x_h - x_{a_2} &= -f' \frac{a'_1(R \sin(\varphi_h) \cos(\theta_h) - X'_S) + b'_1(R \sin(\varphi_h) \sin(\theta_h) - Y'_S) + c'_1(R \cos(\varphi_h) - Z'_S)}{a'_3(R \sin(\varphi_h) \cos(\theta_h) - X'_S) + b'_3(R \sin(\varphi_h) \sin(\theta_h) - Y'_S) + c'_3(R \cos(\varphi_h) - Z'_S)} \\ y_h - y_{a_2} &= -f' \frac{a'_2(R \sin(\varphi_h) \cos(\theta_h) - X'_S) + b'_2(R \sin(\varphi_h) \sin(\theta_h) - Y'_S) + c'_2(R \cos(\varphi_h) - Z'_S)}{a'_3(R \sin(\varphi_h) \cos(\theta_h) - X'_S) + b'_3(R \sin(\varphi_h) \sin(\theta_h) - Y'_S) + c'_3(R \cos(\varphi_h) - Z'_S)} \end{aligned} \quad (26)$$

In order to obtain a unique solution by LSM, the unequal condition $2(N + N') > (N + N' + 3)$ must be formatted.

Where N and N' denote the amount of the observed points in the left and right image planes.

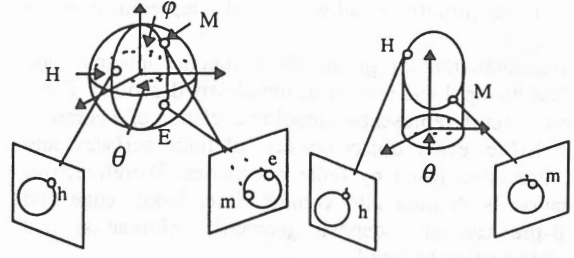


Fig. 13. Conic curve feature. Fig. 14. Intersection curve feature.

B.2) Intersection curve feature

Another kind of important linear feature is intersection curve. Let us take a plane intersecting with a cylinder as an example to derive the mathematical model. We also get

$$x_h - x_o = -f \frac{a_1(X_H - X_S) + b_1(Y_H - Y_S) + c_1(Z_H - Z_S)}{a_3(X_H - X_S) + b_3(Y_H - Y_S) + c_3(Z_H - Z_S)} \quad (30a)$$

$$y_h - y_o = -f \frac{a_2(X_H - X_S) + b_2(Y_H - Y_S) + c_2(Z_H - Z_S)}{a_3(X_H - X_S) + b_3(Y_H - Y_S) + c_3(Z_H - Z_S)} \quad (30b)$$

$$\begin{aligned} x_H &= R \cos(\theta) \\ y_H &= R \sin(\theta) \end{aligned} \quad (31)$$

$$z_H = A'R \cos(\theta) + B'R \sin(\theta) + D'$$

Where: A, B, C are components of the normal vectors of the plane; D is a constant; R is a radius of cylinder, θ indicate a parameter, $A' = A/C$, $B' = B/C$, $D' = D/C$. In the same way, we can obtain equation for the point w (non-corresponding to point h) in the right image.

No matter many points are measured on the intersection linear feature in the left or right images, only one unknown θ is added. Thus if the unequal condition $(N + N') > 4$ is met, the unique solution can be obtained by LSM.

We here only discussed the mathematical models for straight line, intersection curve, and sphere. Others such as spheroid, parabola, hyperbola and sweeping can similarly be processed. These detail discusses can be located in [Zhou 1994].

C) Experiments

Simulation: The simulated images are generated by back-projection. The camera parameters including interior parameters and exterior parameters are designed. The industrial objects are constructed by combining CSG and B-pre with GEMS data structure. The size of all simulated images without any noise are 200×200 pixels, with a pixel size of 50 um. In simulation, we divide experiments into four groups. The first group is to reconstruct cube using straight line. The second group is to reconstruct regular solid using conic curves. The third group is to reconstruct intersected objects by two primitives using intersection edges. The fourth group is to reconstruct complex objects by comprehensive usage of straight lines, conic curves, intersection curves.

(1) The geometric elements for the cube (length, width, and height) are shown in table 4. Figures 15a, 15b are a stereo pair, and figure 15c is its 3D reconstruction drawing.

(2) The geometric elements (radius, height, semi-major axis, semi-medium axis, semi-minor axis) for sphere, cylinder, spheroid are shown in table 5, table 6, table 7. Figures 16a, 16b, 17a, 17b, 18a, 18b are the stereo pairs for sphere, cylinder, and spheroid. Figure 16c, 17c, 18c are their 3D reconstructions.

(3) The geometric elements (radius, height, other parameter) for intersection of a plane and a cylinder, a sphere and a sphere as well as a cylinder and a cylinder are shown in table 8, table 9,

table 10. Figures 19a, 19b, 20a, 20b, 21a, 21b are their stereo pairs. Figures 19c, 20c, 21c are their 3D reconstruction drawings.

(4) The geometric elements (radius, height, other parameter) of the complex object are shown in table 11. Figures 22a, 22b are a stereo pair. Figure 22c is its 3D reconstruction.

Table 4 (Cube) (T. = theoretic, C. = Calculable, and V. = Value.)

Length (mm)		Width (mm)		Height (mm)	
T. V.	C. V.	T. V.	C. V.	T. V.	C. V.
1000.0	999.983	1000.0	1000.066	1000.0	1000.107

Table 5 (sphere)

Radius (mm)	
T. V.	C. V.
800.0	799.9906

Table 6 (Cylinder)

Radius		Height	
T. V.	C. V.	T. V.	C. V.
600.0	599.9391	800.0	800.3074

Table 7 (Spheroid)

Semi major axis (A)		Semi medium axis (B)		Semi minor axis (C)	
T. V.	C. V.	T. V.	C. V.	T. V.	C. V.
1200.0	1200.001	400.00	400.002	1000.0	999.9353

Table 8 (intersection of plane and cylinder)

Radius		A'		B'		D'	
T. V.	C. V.	T. V.	C. V.	T. V.	C. V.	T. V.	C. V.
800.0	800.01	-0.50	-0.501	-0.50	-0.5096	1000.0	1000.1

Table 9 (intersection of sphere and sphere)

Big sphere radius		Small sphere radius		Height	
T. V.	C. V.	T. V.	C. V.	T. V.	C. V.
800.0	799.9918	400.0	400.0991	100.0	100.0732

Table 10 (intersection of cylinder and cylinder)

Big cylinder radius		S. cylinder radius		Height	
T. V.	C. V.	T. V.	C. V.	T. V.	C. V.
600.00	600.0076	450.00	450.0398	0.00	-0.06732

Table 11 (a complex object)

Primitive Name	Parameters Name	D. V. (mm)	C. V. (mm)	
Cube	length	600.0	600.019	
	width	400.0	399.815	
	height	200.0	199.992	
Frustum of cone	up radius	100.0	100.101	
	down radius	200.0	200.203	
	height	300.0	299.901	
	translation parameters	Xo	0.00	-
		Yo	0.00	-
		Zo	0.00	-
	rotation parameters	F	0.00	-
V		0.00	-	
K		0.00	-	
(Hole) Cylinder	radius	100.0	99.989	
	height	300.0	299.331	
	translation parameters	Xo	0.00	-
		Yo	0.00	-
		Zo	0.00	-
	rotation parameters	F	0.00	-
		V	0.00	-
	K		0.00	-

(Continue table 11)

Parameter	First cylinder (mm)		Second cylinder (mm)	
	D.V.	M. V.	D.V.	M. V.
Radius	200.00	199.694	100.00	99.889
Height	200.00	199.896	200.00	200.218
Transfer	0.00	0.01	200.00	200.031
	0.00	0.14	200.00	

	0.00	0.26	-200.00	-200.307
Rotate	0.00	-	0.00	-
	0.00	-	0.00	-
	0.00	-	0.00	-

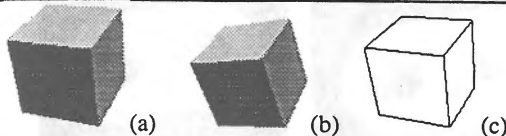


Fig. 15. A cube and its reconstruction.

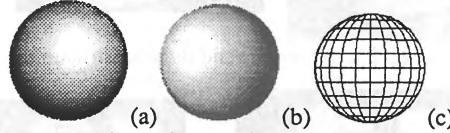


Fig. 16. A sphere and its reconstruction.

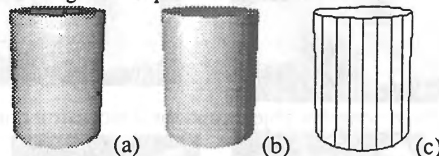


Fig. 17. A cylinder and its reconstruction.

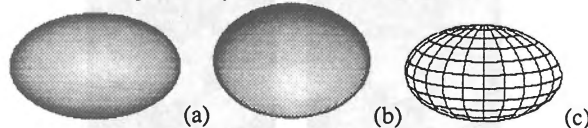


Fig. 18. A spheroid and its reconstruction.

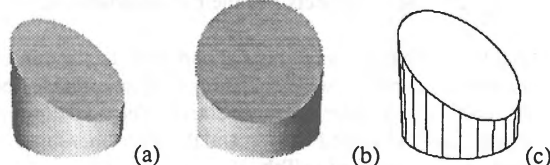


Fig. 19. A plane and a cylinder intersection and its reconstruction.

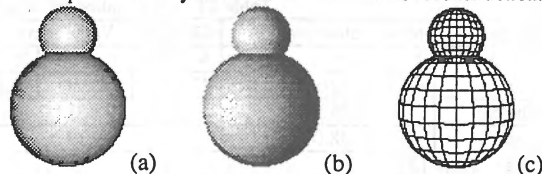


Fig. 20. A sphere and a sphere intersection and its reconstruction.

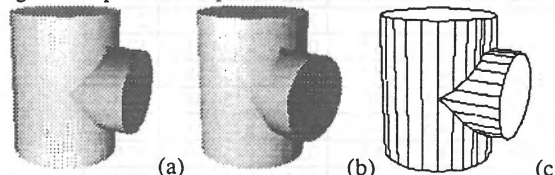


Fig. 21. A cylinder and a cylinder intersection and its reconstruction (where: Great Cylinder Equation $X=R\cos(u), Y=R\sin(u), Z=t$, Small Cylinder Equation $X=R'\cos(u), Y=t', Z=R'\sin(u)$, Central axis for small cylinder is consistent with y-axis of great cylinder).

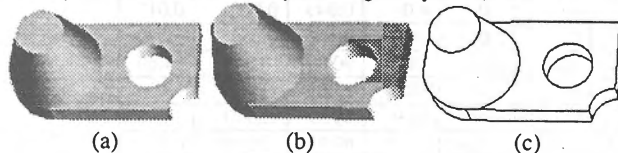


Fig. 22. A complex object and its reconstruction.

Experiments: Three groups of real datum (images) are tested. The first group is composed of an object; the second image has three objects; and the third image contains many objects. The size of images is 512×512 pixels with 8 bit/256 gray level. These industrial parts are designed by GEMS system, and then are manufactured in factory. Finally these objects are put in experimental platform. Three groups of real images are captured by CCD camera (type: COSMICAR) when the cameras was

located with a depth distance about 880mm long. The reconstructed objects are drawn by wire draw, which overlap with original image. As illustrated in figures 23, 24, 25.

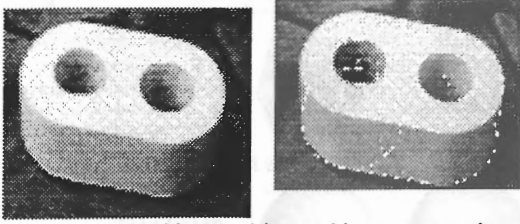


Fig. 23. An object and its reconstruction.

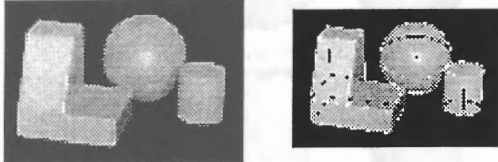


Fig. 24. Three complex objects and their reconstructions.

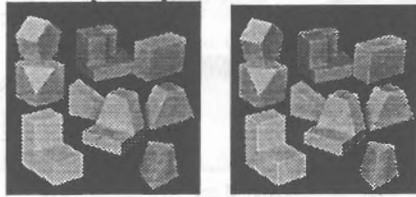


Fig. 25. Many objects and their reconstructions.

The final tested object is an industrial part from factory. In order to evaluate the precision, we calculate the 3D coordinates of 16 vertices and a cylinder's parameters. The 3D practical coordinates are measured by manual. The measured and calculated values are listed in Tab. 12.

Table 12 (a real industrial object)

Parameter	Mea. Value (cm)			Calculated Value (cm)		
	X	Y	Z	X	Y	Z
Coordinate of center	45.5	130.0	0.0	45.53	130.71	-0.126
Radius/cm	23.50			23.51		
Height/cm	38.00			38.89		

(Continue table 12)

	Measured Value(cm)			Calculated Value (cm)		
	X	Y	Z	X	Y	Z
1	0.0	154.5	38.0	0.03	154.51	37.89
2	21.0	154.5	38.0	21.04	154.58	37.65
3	21.0	154.5	0.0	0.03	154.48	0.04
4	0.0	154.5	0.0	21.04	154.51	0.15
5	69.0	154.5	38.0	0.03	154.50	37.91
6	91.0	154.5	38.0	21.04	154.48	37.86
7	91.0	154.5	0.0	0.03	154.49	0.04
8	69.0	154.5	0.0	21.04	154.53	0.08
9	91.0	0.0	0.0	91.13	0.095	0.086
10	0.0	0.0	0.0	0.049	0.000	0.012
11	0.0	0.0	38.0	0.136	0.054	37.79
12	91.0	0.0	38.0	90.89	-0.061	37.69
13	21.0	130.0	38.0	21.09	129.94	38.04
14	69.0	130.0	38.0	69.39	130.41	38.40
15	69.0	130.0	0.0	69.08	130.19	0.01
16	21.0	130.0	0.0	21.09	130.07	-0.05

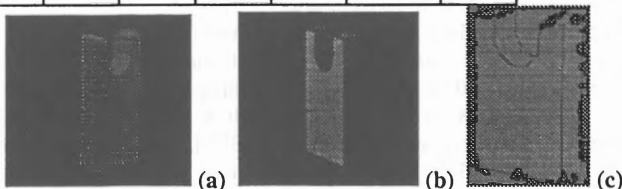


Fig. 26. A practical object and its reconstruction.

D) Conclusion

Reconstruction using line photogrammetry for locating industrial objects in robot vision has apparently advantages. Firstly, since all linear features are described with parametric equations and each entire object is represented by GEMS data structure, the unknown parameters, which describe primitives, can directly be solved. Secondly the mathematical models require the matches are established in not only 2D to 2D, but also 2D to 3D. Thirdly output results are still digital form. Digital output can directly feedback to GEMS systems. Thus this method make it possible the operator can interact between GEMS systems and robot vision. Fourthly, to my algorithm, two camera positions can be permitted with a large angle (see Fig. 13, 21). It means that overlap degree of two images is much less than conventional aerial stereo pair.

5. CONCLUSION

Photogrammetrists can use photogrammetric geometry to solve some of problems, which computer vision scientists are exploring. Hope photogrammetrists can play a wide role in computer vision, robot vision and other fields.

ACKNOWLEDGEMENTS

I want to thank my colleagues of Dept. of Computer Science and Technology at Tsinghua University for their contributions to SIVE, especially Prof. Yu Zhihe (from America). The SIVE system was designed by our vision research group.

REFERENCES

- H. H. Chen, and Huang, T.S., 1990. Matching 3-D line segments with applications to multiple object motion estimation. *IEEE Tran. on PAMI*, 12 (9), pp. 1002-1008.
- Shuyuan Chen and W. H. Tsai, 1991. A systematic Approach to Analytic Determinate of Camera Parameters by Line Features, *Pattern Recognition*, Vol. 23, pp. 859-877.
- H. L. Chou and W. Tsai, 1986. A new approach to robot location by house corners, *Pattern Recognition*, Vol. 19, pp. 439-451.
- Wenhao Feng, 1986. the principal of close-range photogrammetry, *Surveying and Mapping Press*.
- R. M. Haralick and Y. H. Chu, 1984. Solving camera parameters from the prospective project of a parameterized curvature, *Pattern Recognition*, Vol. 17, pp. 637-645.
- Kim, Y.C., Aggarwal, J.K., 1987. Determining object motion in a sequence of stereo images, *IEEE J. of Robotics and Automation*, 3 (6), 599-614.
- Liu, Y. and Huang, T.S., 1988. Estimation of rigid body motion using straight line correspondences. *Computer Vision, Graphics, and Image Processing*, 43, pp. 37-52.
- A. Mitche, S. Seida, and J:K Aggarwal, 1988. Interpretation of structure and motion using straight line correspondence, in *Int. C. of Pattern Recognition*, France, Oct., pp. 1110-1112.
- Z. Ren, 1991. CAD/CAM Principle, Tsinghua University Press.
- Spetsakis, E., Aloimonos, Y., 1990. Structure from motion using line correspondences, *Int. J. of computer vision*, 4, pp. 171-183.
- Sun, Jiaguang, etc., 1989. Data Structure for Geometric Modeling, *Journal of Computer*, No. 3, pp. 181-193.
- Y. Tsai, 1987. A versatile Camera Calibration Technique for High-Accuracy 3D Machine Vision Metrology Using Off-the-Shelf TV Camera and Lenses, *IEEE Robotics and Automation*, Vol. 3, No. 4, pp. 323-244.
- J. Huang, Weng T.S., and Ahuja, N., 1992. Motion and structure from line correspondences: closed form solution, uniqueness, and optimization. *IEEE Tran. on PAMI*, 14 (3), pp. 318-336.
- Z. Yu, 1995. Vision system with Multiple sensors for Space Intelligent Robot, *Technical Handbook*, Dept. of Computer Sci. and Tech. at Tsinghua University.
- G. Zhou, 1994. CAD-based Line Photogrammetry for Automatic Measurement and Reconstruction of Industrial Object. Ph.D. dissertation, Wuhan Technical Univ. of Surveying and Mapping.